Optics Letters

Ultraviolet polarized light emitting and detecting dual-functioning device based on nonpolar n-ZnO/i-ZnO/p-AlGaN heterojunction

Jiangnan Dai,[1,*] Jingwen Chen,[1] Xiaohang Li,[2] Jun Zhang,[1] Hanling Long,[1] Haochung Kuo,[3] Yunbin He,[4] and Changqing Chen[1]

[1]Wuhan National Laboratory for Optoelectronics, Huazhong University of Science and Technology, Wuhan, 430074, China
[2]King Abdullah University of Science and Technology (KAUST), Advanced Semiconductor Laboratory, Thuwal 23955, Saudi Arabia
[3]Department of Photonics and Institute of Electro-Optical Engineering, National Chiao Tung University, 1001 Ta Hsueh Road, Hsinchu 300, Taiwan
[4]Hubei University, Wuhan, 430062, China
*Corresponding author: daijiangnan@hust.edu.cn

Received 9 January 2019; revised 1 March 2019; accepted 4 March 2019; posted 12 March 2019 (Doc. ID 356963); published 5 April 2019

We report on the demonstration of a 386 nm light emission and detection dual-functioning device based on nonpolar *a*-plane n-ZnO/i-ZnO/p-$Al_{0.1}Ga_{0.9}N$ heterojunction under both forward and reverse bias. The electroluminescence intensity under reverse bias is significantly stronger than that under forward bias, facilitated by carrier tunneling when the valence band of p-AlGaN aligns with the conduction band of i-ZnO under reverse bias. Also amid reverse bias, the photodetection was observed and applied in a duplex optical communication device. Optical polarization of the light emission is studied for potential polarization-sensitive device applications. The proposed device provides an important pathway for the multifunctional devices operating in a UV spectrum.

https://doi.org/10.1364/OL.44.001944

Luminescence and photodetection can be achieved in two separate devices; yet each often requires a more complex circuit construction and fabrication process. Therefore, it is desirable to integrate both functions in a single monolithic device and enable technically important multifunctional electronics. The dual-functioning device operating in a visible spectrum has been fabricated with a light-responsive double-heterojunction nanorod based on CdS, CdSe, and ZnSe nanocrystal materials [1]. Benefitting from a high exciton binding energy (60 meV) and large direct bandgap (3.37 eV) [2], ZnO is a promising candidate for UV light emitting diodes (LEDs), detectors, and sensors [3]. Considering the unavailability of the *p*-type ZnO [4], as well as the small lattice mismatch (~1.8%) and similar band structure between ZnO and GaN [5], p-GaN has been widely employed to fabricate heterojunction devices with *n*-type ZnO. As for LEDs based on n-ZnO/p-GaN, the emission from the p-GaN layer generally dominates the spectrum, because the majority of the depletion region lies in p-GaN [6], causing a low carrier injection efficiency in ZnO.

In this Letter, we propose a feasible solution to improve the carrier injection and radiative recombination efficiencies by inserting an intrinsic ZnO (i-ZnO) layer between the n-ZnO and p-AlGaN, all on the nonpolar $(11\bar{2}0)$ *a*-plane, where the depletion region almost entirely resides in the i-ZnO layer [7]. By increasing the conduction band offset ΔE_c, the proposed heterojunction with p-AlGaN can greatly hinder the electron leakage to the *p*-type layer, thus localizing electrons and improving carrier injection efficiency in i-ZnO [8]. Moreover, compared to polar ZnO, nonpolar ZnO can realize polarized emission or detection, arising from modification of the valence band structure caused by anisotropic in-plane strains and the hexagonal unit cells distortions [9]. This unique property makes nonpolar ZnO feasible to fabricate polarization-sensitive optoelectronic devices, such as polarized sensors and detectors. In previous reports, the luminescence under forward bias and detection under reverse bias of a p-AlGaN/i-ZnO/n-ZnO (PIN) structure device were reported [10]. As for luminescence under reverse bias, only avalanche-mechanism-based luminescence under reverse bias was explained in detail [8]. In this Letter, luminescence mechanisms based on a tunneling effect, as well as a light detection mechanism, were studied in detail through experiments and simulation. Furthermore, the polarized luminescence of the heterojunction UV-LEDs was studied by angle-resolved electroluminescence (EL) and photoluminescence (PL) measurements.

To form PIN heterojunction, a 2.2 μm *p*-type AlGaN layer was first grown by metal organic chemical vapor deposition at 1030°C on *a*-plane aluminum nitride (AlN) templates on *r*-plane sapphire. The concentration and mobility of a hole in the p-$Al_{0.1}Ga_{0.9}N$ layer are 3.8×10^{17} cm^{-3} and 8.0 cm^2/Vs, determined by Hall measurements, respectively. The nonpolar 200 nm i-ZnO and 150 nm n-ZnO (Al-doped ZnO, i.e., AZO) layers were grown on the p-AlGaN layer by using pulsed laser deposition at 700°C. The layer thickness and growth orientation were verified by a transmission electron microscope (TEM), as shown in Fig. 1(d). The unintentional doping

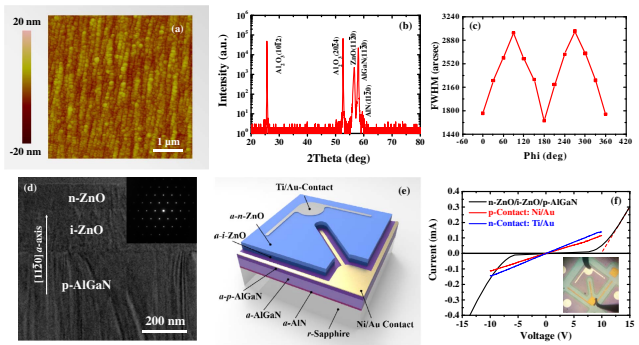

Fig. 1. (a) AFM image, (b) XRD $2\theta - \omega$ spectra, and (c) XRD rocking curve FWHMs as a function of the azimuthal angle φ for the heterojunction. (d) Cross TEM image of the heterojunction with the SAED pattern inside. (e) Structure schematics and (f) $I - V$ curves of the PIN heterojunction. The inset figure in (d) shows the top-view photo of the device under electrical injection.

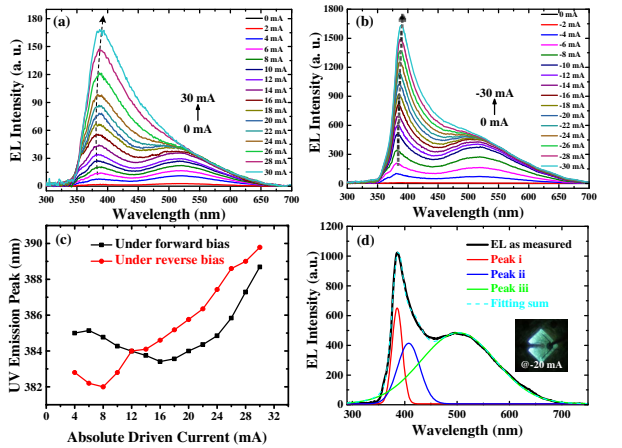

Fig. 2. RT on-wafer testing EL spectra for the device working in the LED mode under various (a) forward biases and (b) reverse biases with the injection current ranging from −30 to 30 mA. (c) UV emission peak at various injection currents. (d) Peak resolving of the EL from the heterojunction at −20 mA.

concentration of i-ZnO is 5.6×10^{15} cm^{-3}. The electron concentration and mobility of n-ZnO are 3.2×10^{20} cm^{-3} and 16.5 cm^2/Vs, respectively. The surface morphology of the PIN heterojunction wafer was characterized by atomic force microscopy (AFM), as shown in Fig. 1(a). The RMS surface roughness over 5×5 μm^2 is 1.94 nm. The crystallinity of the deposited films was probed by a high-resolution x-ray diffraction system ($\lambda = 1.5406$ Å). As shown in Fig. 1(b), only $(11\bar{2}0)$ peaks at 56.5° and 57.9° belonging to the *a*-plane ZnO and AlGaN can be observed, confirming the nonpolar structure. The threading and stacking fault dislocation densities of the ZnO layer were estimated [11] to be about 1×10^{11} cm^{-2} and 1×10^6 cm^{-1}, according to Fig. 1(c).

The heterojunction devices with dimensions of 400×400 μm^2 were fabricated and shown in Fig. 1(c). Ti/Al (20/40 nm) and Ni/Au (30/60 nm) were deposited on n-ZnO and p-AlGaN, respectively, and further annealed at 500°C for 1 min in the N_2 ambient to form ohmic contact, verified by Fig. 1(d). The large forward turn-on voltage of 10 V is due to the extra series resistance caused by the intrinsic ZnO layer, as presented in Figs. 2(a) and 2(b). The EL exhibits an obvious UV emission peak at 386 nm with a broad defect-related emission located at around 505 nm. As shown in Fig. 2(a), for the device under forward bias, slight UV emission peak blueshift due to a band-filling effect [12,13] and redshift due to a raised junction temperature at a higher current can be found with increasing injection current. The competition between the band-filling and thermal excitation effects was also observed for the device under reverse bias. However, the redshift happened earlier (about $|-8|$ mA) than the forward bias mode (16 mA), because carriers are less likely to be confined at the p-AlGaN/i-ZnO and i-ZnO/n-ZnO, which led to a weaker band-filling effect. Notably, the intensity of UV emission under reverse bias is nearly 10 times larger than that under forward bias at the same injection current, and the FWHM of the emission peak is almost reduced by half. Figure 2(d) shows the room temperature (RT) EL spectra of reverse-biased PIN heterojunction at 20 mA with the fitted peaks. Considering that the EL spectra cannot be fitted well by only two peaks, three peaks are set to resolve the spectra. The Peak *i* at around 386 nm is confirmed to be from the near-band-edge (NBE) emission of the i-ZnO layer [8]. The inset image of Fig. 2(d) showed uneven illumination because the carrier mobility of *p*-type and *i*-type layer materials is not high, resulting in uneven current spreading. Using built-in potential $\varnothing_i = 0.521$ eV, applied voltage $V_a = -40$ V, $d = 200$ nm, $\varepsilon_{sn} = 7.9 \times 10^{-12}$ F/m, and $\varepsilon_{sp} = 10.274 \times 10^{-12}$ F/m, the total depletion layer width x_d is

$$x_d = x_n + x_p + x_i = \sqrt{d^2 + \frac{2\varepsilon_{sn}\varepsilon_{sp}}{q}\frac{(N_a + N_d)^2(\phi_i - V_a)}{N_a N_d(N_a\varepsilon_{sp} + N_d\varepsilon_{sn})}} = 231 \text{ nm}. \quad (1)$$

Then the depletion width in p-AlGaN was calculated to be nearly 31 nm, which is much lower than 200 nm of i-ZnO, inferring that the majority of the depletion region lies in i-ZnO.

Figure 3 illustrates the light emitting and detecting mechanisms of the reverse-biased device. Some of the injected

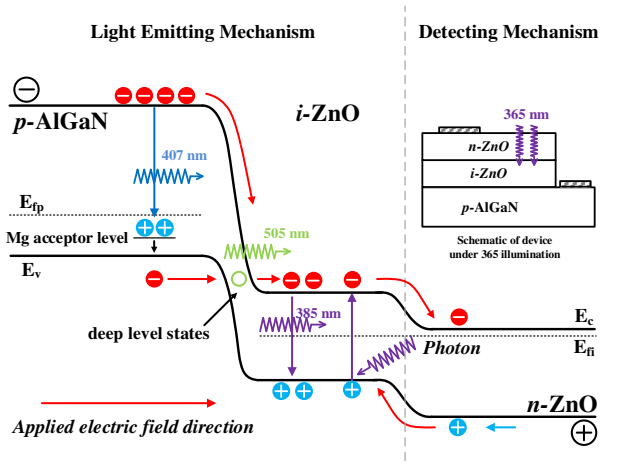

Fig. 3. Energy band diagram of the proposed dual-functioning device under large reverse bias for dual-mode operation.

electrons drift across the p-AlGaN arriving at the AlGaN/ZnO interface, and others from shallow donors recombine with holes in the Mg deep acceptor levels in the p-AlGaN to produce Peak ii at 407 nm, consistent with Refs. [12,13]. For the electrons arriving at the interface, part of them may be captured by the oxygen vacancy-related deep-level states near the interface, yielding the broad Peak iii at around 505 nm [14]. Meanwhile, valence electrons in p-AlGaN can tunnel to the conduction band of i-ZnO and recombine with holes, producing the sharp Peak *i* at 386 nm (ZnO NBE emission). The electrons from p-AlGaN can tunnel through the thin barrier to i-ZnO, because the Fermi levels of p-AlGaN and i-ZnO gradually separate, and the occupied valence band of the p-AlGaN is at the same level or higher than the unoccupied conduction band of the i-ZnO with the increasing of reverse voltage. Under forward bias, holes and electrons are concentrated at the interface of p-AlGaN/i-ZnO and i-ZnO/n-ZnO, respectively, leading to a low overlap ratio of electron-hole wave function and low radiative recombination efficiency, since the i-ZnO layer is thick. Under reverse bias, holes can tunnel through the i-ZnO/n-ZnO interface into i-ZnO and be amplified by the impact ionization [15], which greatly improves the EL intensity by ~10 times, indicating higher external quantum efficiency, which was not measured, but expected to be low which deserves further improvement.

To clarify the carrier tunneling behavior, the band diagram and carrier concentration at −127 V were simulated by Crosslight APSYS. Since a perfect semiconductor was used in the model, the reverse operating voltage of the device was much higher than the experimental value which was based on the semiconductor material with a lot of defects. The wide interface gap between p-AlGaN and n-ZnO made the electron and hole concentrations in i-ZnO almost zero, while the carrier tunneling happened when the voltage decreased to −127 V′ the concentrations of the electron and hole increased to a scale of 10^{11} cm^{-3}. Considering that the carriers were injected from electrodes at p-AlGaN and n-ZnO, the carriers in i-ZnO could only be explained as the tunneling effect, where the electrons tunneled from p-AlGaN, and the holes from tunneled from n-ZnO. The 378 nm NBE emission shown in the inset image of Fig. 4(b) can also prove the carrier tunneling and recombination behavior. To clarify the impact ionization amplification of the carrier, the simulation result not considering the impact ionization (light on only) was carried out. Under the influence of impact ionization, the light emission intensity was significantly enhanced [Fig. 4(d)]. Figure 4(e) showed that the hole concentration in i-ZnO has increased by more than 1000 times and should be responsible to the emission enhancement.

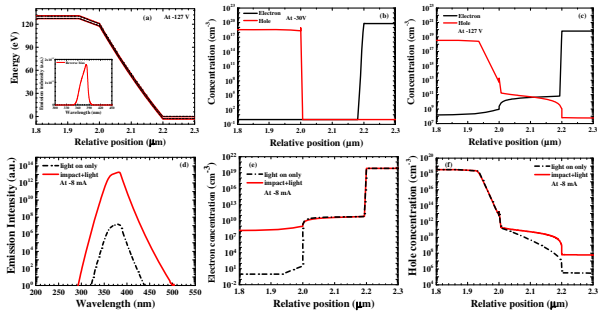

Fig. 4. Under reverse bias, (a) the band diagram at −127 V with an inset image about the emission spectrum, and the carrier concentration distributions at (b) −30 V and (c) −127 V. (d) Emission spectrum, and (e) electron and (f) and hole concentration of the PIN heterojunction under light considering or not considering the impact ionization effect.

Considering the wide bandgap of ZnO and AlGaN, an extremely large reverse bias (normally >500 V) is required to have the impact ionization effect for a reverse-biased PN diode, which is accompanied with very large current flow. In this case, significant current flow and light emission were obtained when the reverse bias exceeds 5 V [see Fig. 1(d)], indicating that the interband tunneling process occurred, and this promoted the carrier multiplication. The numerical calculations also presented that the impact ionization effect was essential to the current flow at reverse bias.

As shown in Fig. 5(a), an obvious photocurrent was observed when the heterojunction was excited by 365 nm light. 94.2% of the excited light was absorbed by n-ZnO [16], and the others were absorbed by i-ZnO. Although a low electric field existed in the n-ZnO layer, the photo-generated electron-hole pairs could be collected and amplified because of the tunneling and impact ionization effect. The photocurrent is 0.946 mA at −50 V, while the dark current was 14.748 mA, and obvious light emission can be observed. This emission and detection dual-function make this heterojunction be able to realize duplex optical communication. Through definition of the binary 0 and 1 of emission and detection, as shown in Fig. 5(b), the heterojunction can also decode the received illumination information while transmitting the information in real time, completely free of crosstalk. This demo of duplex communication can be viewed and experienced in the supplemental material Code 1, Ref. [17]. Compared to normal forward-biased LEDs, this proposed reverse-biased LED can work as a photodetector simultaneously and shows a wider application scenario.

During EL and PL measurements, a Glan–Taylor prism was placed between the sample and the photodetector to resolve the optical polarization anisotropy [18], showing the result in Figs. 5(c) and 5(d). Usually, emitted light with an electric vector perpendicular ($E \perp c$) and parallel ($E \| c$) to the *c*-axis of

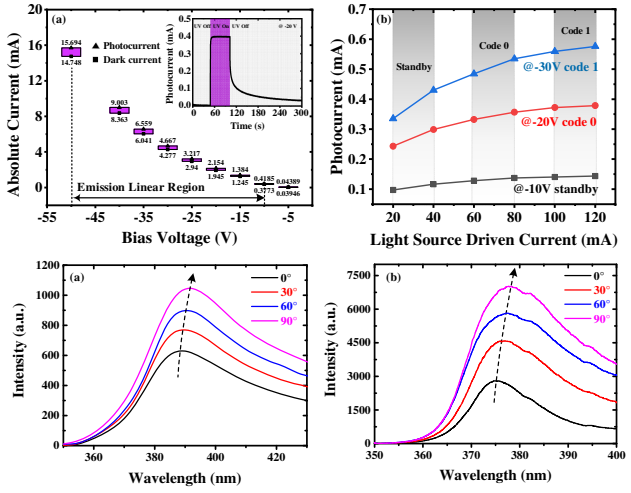

Fig. 5. (a) Dark current and photocurrent of a reverse-biased heterojunction with emission simultaneously. (b) Photo-generated current under light excited with different intensities. (c) Angle-resolved EL spectra of the device at −20 mA. (d) Angle-resolved PL spectra.

the *a*-ZnO crystal is defined as transverse electric (TE) and transverse magnetic (TM) modes, respectively [19]. The TE and TM modes originate from transitions between the conduction band and the heavy-hole band, as well as the crystal field splitting band. When the angle between the prism polarization direction and the c-axis of *a*-ZnO was changed from 0° to 90°, ~3 nm redshifts of the EL and PL emission peak are observed, indicating that the peak wavelength of the TE modes are consistently larger than those of the TM modes, because the topmost valence band has not switched to the crystal field splitting band. The degrees of polarization (DOPs, i.e., ρ) [20] of the EL and the PL are 0.23 and 0.33, respectively. Similar to the Al(In)GaN material, the DOP of the LED with ZnO active layer decreases as the temperature rises, because the holes increasingly occupy deeper split-off valence bands, leading to stronger TM light [21]. The lower DOP of EL than that of PL in this Letter results from the heating caused by electrical injection. Ascribed to the polarized emission and detection characteristics, through modulation of the polarized information of the incident light, it is possible to double the bandwidth of data receiving of this duplex optical communication device.

In summary, the nonpolar *a*-plane n-ZnO/i-ZnO/p-$Al_{0.1}Ga_{0.9}N$ dual-functioning heterojunction was fabricated and investigated. A sharp UV emission peak at around 386 nm for the PIN heterojunction was observed in the EL spectra under both forward and reverse bias. The EL emission under the reverse bias results from the recombination of electron tunneling from p-AlGaN to i-ZnO and holes ionized in i-ZnO layer. Photoresponse to the 365 nm light was observed indicating the possible duplex optical communication device. The polarized luminescence of the PIN was also studied, and we obtained the polarized light with the DOPs of 0.23 and 0.33 for the EL and the PL spectra, respectively. The proposed dual-functioning nonpolar heterojunction device under reverse bias provides a valuable basis for the structural design of multifunctional electronics.

Funding. Key Project of Chinese National Development Programs (2016YFB0400804); Key Laboratory of Infrared Imaging Materials and Detectors; Shanghai Institute of Technical Physics, Chinese Academy of Sciences (CAS) (IIMDKFJJ-17-09); National Natural Science Foundation of China (NSFC) (11574166, 61377034, 61675079, 61774065); KAUST Baseline (BAS/1/1664-01-01); KAUST Competitive Research (URF/1/3437-01-01); GCC Research Council (REP/1/3189-01-01); Director Fund of WNLO.

Acknowledgment. The authors acknowledge the numerical calculations conducted by Prof. Zi-Hui Zhang at the Hebei University of Technology.

REFERENCES

1. N. Oh, B. H. Kim, S. Cho, S. Nam, S. P. Rogers, Y. Jiang, J. C. Flanagan, Y. Zhai, J. Kim, J. Lee, Y. Yu, Y. K. Cho, G. Hur, J. Zhang, P. Trefonas, J. A. Rogers, and M. Shim, Science **355**, 616 (2017).
2. M. H. Huang, S. Mao, H. Feick, H. Q. Yan, Y. Y. Wu, H. Kind, E. Weber, R. Russo, and P. D. Yang, Science **292**, 1897 (2001).
3. X. Y. Liu, C. X. Shan, C. Jiao, S. P. Wang, H. F. Zhao, and D. Z. Shen, Opt. Lett. **39**, 422 (2014).
4. Y. R. Ryu, T. S. Lee, J. H. Leem, and H. W. White, Appl. Phys. Lett. **83**, 4032 (2003).
5. J. N. Dai, X. Y. Han, Z. H. Wu, C. H. Yu, R. F. Xiang, Q. H. He, Y. H. Gao, C. Q. Chen, X. H. Xiao, and T. C. Peng, J. Alloys. Compd. **489**, 519 (2010).
6. Y. I. Alivov, E. V. Kalinina, A. E. Cherenkov, D. C. Look, B. M. Ataev, A. K. Omaev, M. V. Chukichev, and D. M. Bagnall, Appl. Phys. Lett. **83**, 4719 (2003).
7. H. K. Liang, S. F. Yu, and H. Y. Yang, Opt. Express **18**, 3687 (2010).
8. J. Chen, J. Zhang, J. Dai, F. Wu, S. Wang, C. Chen, H. Long, R. Liang, C. Zhao, C. Chen, Z. Tang, H. Cheng, Y. He, and M. Li, J. Phys. D **50**, 115101 (2017).
9. H. Matsui and H. Tabata, Appl. Phys. Lett. **101**, 231901 (2012).
10. C. X. Shan, J. S. Liu, Y. J. Lu, B. H. Li, F. C. C. Ling, and D. Z. Shen, Opt. Lett. **40**, 3041 (2015).
11. A. Chakraborty, K. C. Kim, F. Wu, J. S. Speck, S. P. DenBaars, and U. K. Mishra, Appl. Phys. Lett. **89**, 41903 (2006).
12. M. Jeong, B. Oh, M. Ham, S. Lee, and J. Myoung, Small **3**, 568 (2007).
13. L. Eckey, U. von Gfug, J. Holst, A. Hoffmann, A. Kaschner, H. Siegle, C. Thomsen, B. Schineller, K. Heime, M. Heuken, O. Schön, and R. Beccard, J. Appl. Phys. **84**, 5828 (1998).
14. H. Y. Xu, Y. C. Liu, Y. X. Liu, C. S. Xu, C. L. Shao, and R. Mu, Appl. Phys. B **80**, 871 (2005).
15. Z. Zhang, Y. Zhang, W. Bi, C. Geng, S. Xu, H. V. Demir, and X. W. Sun, Appl. Phys. Lett. **108**, 151105 (2016).
16. J. F. Muth, R. M. Kolbas, A. K. Sharma, S. Oktyabrsky, and J. Narayan, J. Appl. Phys. **85**, 7884 (1999).
17. Application demo for duplex communication, https://doi.org/10.6084/m9.figshare.7791518.
18. J. Chen, J. Zhang, J. Dai, F. Wu, S. Wang, H. Long, R. Liang, J. Xu, C. Chen, Z. Tang, Y. He, M. Li, and Z. Feng, Opt. Mater. Express **7**, 3944 (2017).
19. H. Long, F. Wu, J. Zhang, S. Wang, J. Chen, C. Zhao, Z. C. Feng, J. Xu, X. Li, J. Dai, and C. Chen, J. Phys. D **49**, 415103 (2016).
20. C. Lai, Y. Huang, K. Kou, C. Chen, L. Tu, and S. Feng, Appl. Phys. Lett. **107**, 22110 (2015).
21. T. Kolbe, A. Knauer, C. Chua, Z. Yang, V. Kueller, S. Einfeldt, P. Vogt, N. M. Johnson, M. Weyers, and M. Kneissl, Appl. Phys. Lett. **99**, 261105 (2011).